Supplementary material to: Uncertainties in atmospheric chemistry modelling due to convection parameterisations and subsequent scavenging

H. Tost, M. G. Lawrence, C. Brühl, P. Jöckel,
The GABRIEL Team, The SCOUT-O3-DARWIN / ACTIVE Team

February 16, 2010

1 Uptake of HNO_3 on ice

The importance of the uptake, scavenging and sedimentation of HNO_3 on ice has been analysed with a sensitivity study using the T1 convection scheme, using a lower horizontal and vertical resolution(T42L19). Nevertheless, the effects are similar to the standard simulations and in agreement with previous model studies (e.g., v. Kuhlmann and Lawrence, 2006).

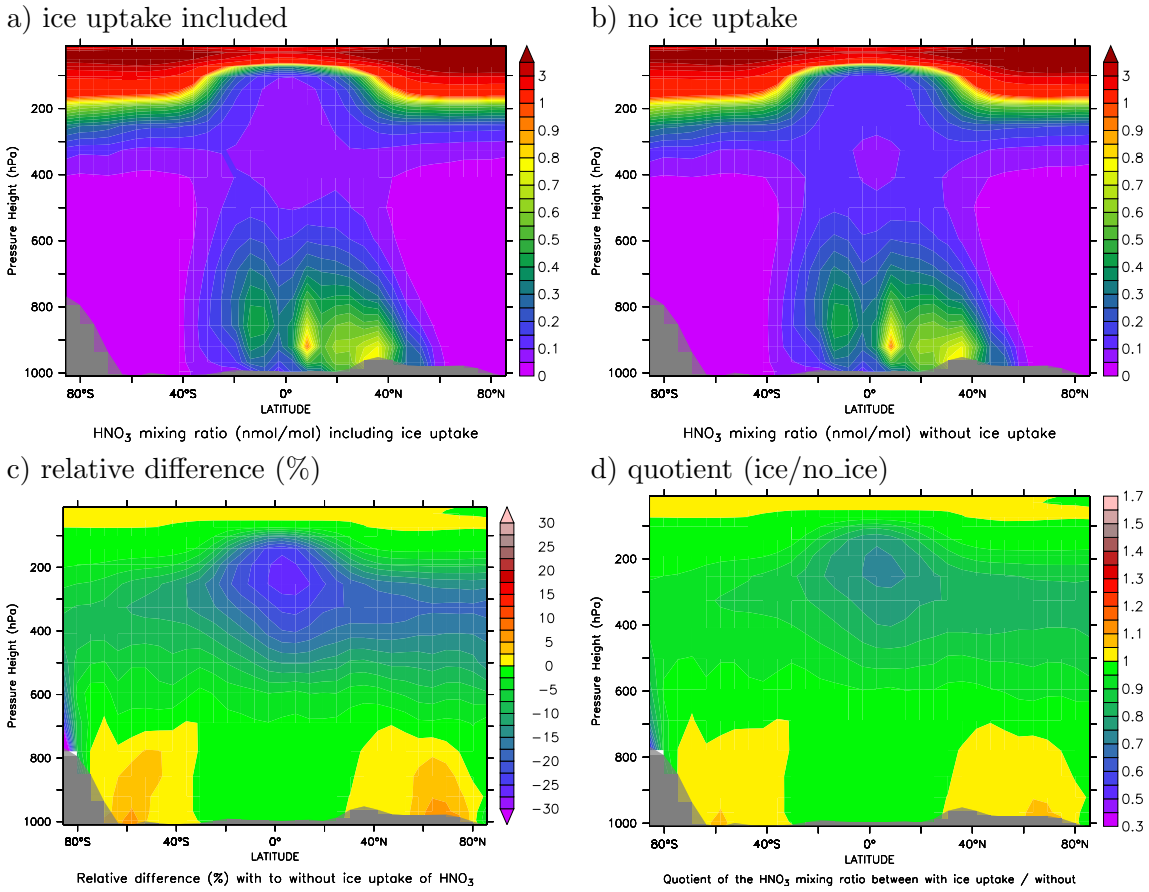

Figure 1: Zonal average HNO_3 in a simulation with ice uptake included (a), with no ice uptake (b) in nmol/mol, the relative difference between the two is shown in c), and the quotient between the two simulations in d).

2 Precipitation at the surface

Even though the surface precipitation has already been analysed by Tost et al. (2006), the simulation setup is slightly different and therefore these figures are shown in this supplement. The patterns are quite similar, only ZHW has lower precipitation (partly due to the reasons explained by Tost et al. (2006)). Compared to CMAP (CPC Merged Analysis of Precipitation) precipitation data for that period, all agree reasonably well.

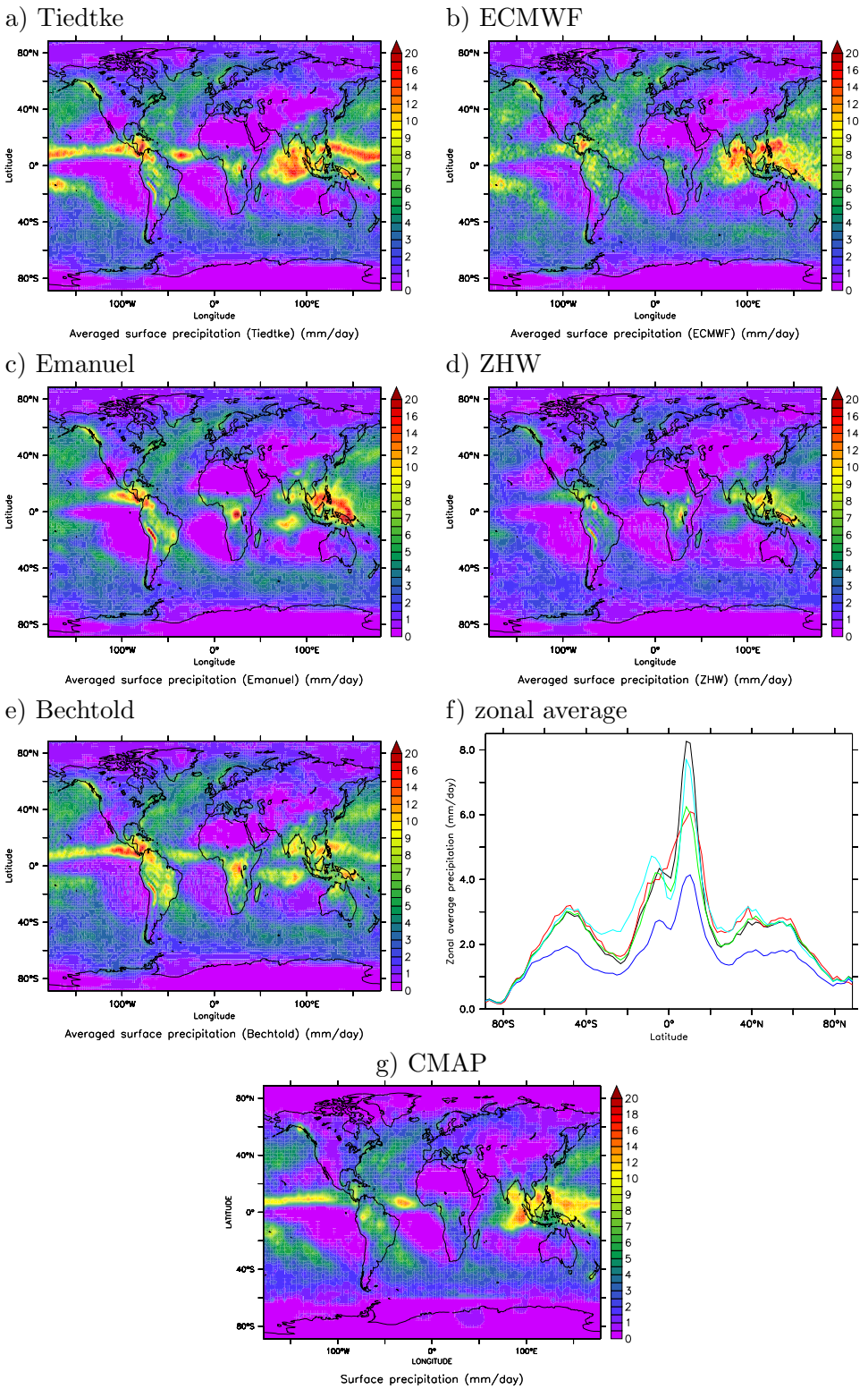

Figure 2: 4 month average of the surface precipitation (both convective and large-scale): a) to e) for the five simulations and f) the zonal average of all simulations. Panel g) depicts the CMAP precipitation for that period.

Table 1: Biases (MODEL - OBS, in mm/day), Pearson's correlation and linear regression ($y = \text{SLOPE} * \text{x} + \text{INTERCEPT}$) for the comparison of the simulations using the different convection schemes with the CMAP precipitation data for that period.

	T1	EC	Ema	ZHW	B1
Bias	0.29	0.35	0.18	-0.53	0.43
R^2	0.71	0.68	0.58	0.54	0.58
Slope	0.89	0.79	0.72	0.46	0.71
Intercept	0.64	0.91	0.88	0.67	1.16

3 Outgoing long-wave radiation at the top of the atmosphere (OLR)

Since the radiation budget must not be substantially altered by an exchange of the convection scheme, the convection schemes have been tuned to achieve realistic outgoing long-wave radiation. This is shown in these figures, comparing to NOAA radiation data in panel f).

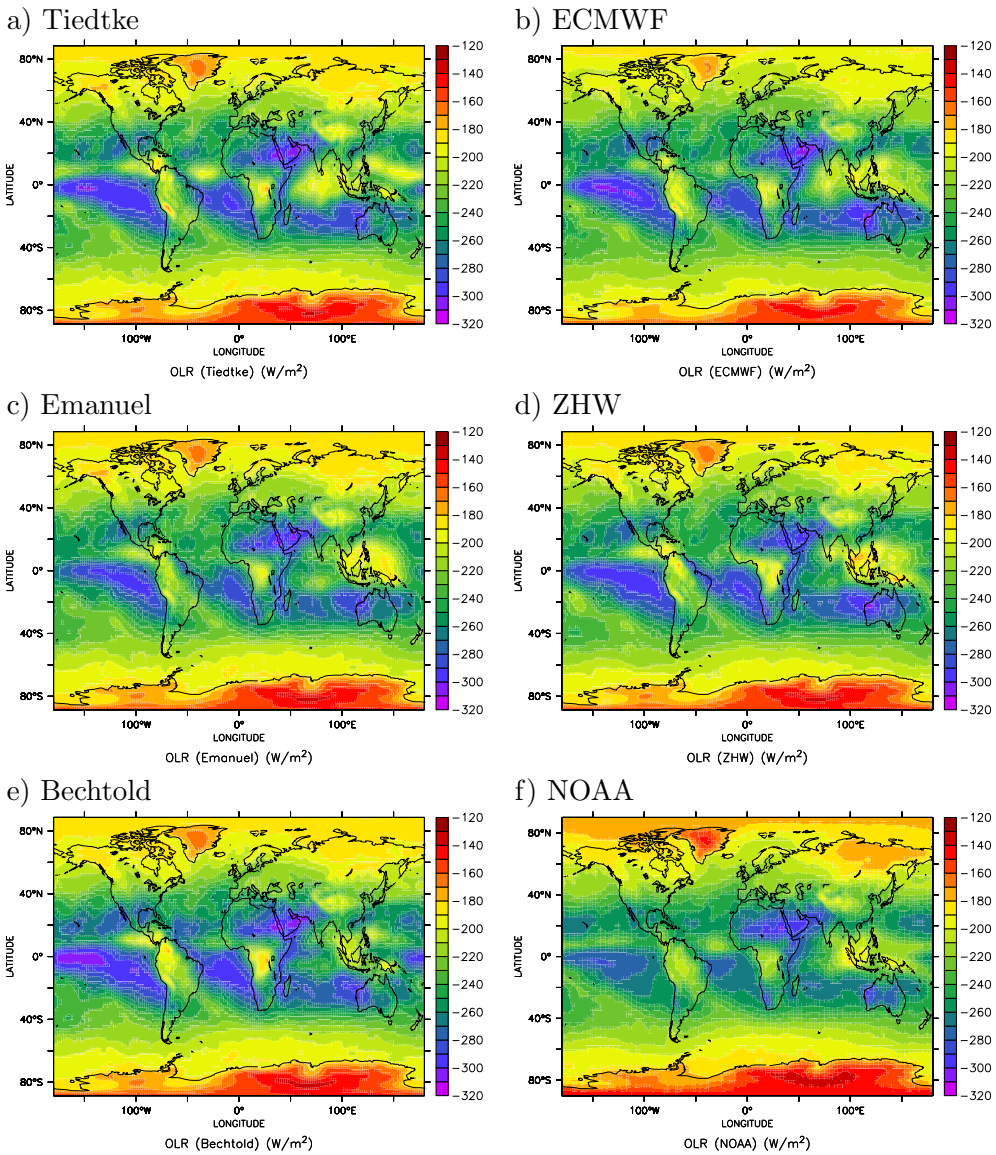

Figure 3: 4 months average of the outgoing long-wave radiation (top of the atmosphere) for the five simulations (a) to e)) and from the NOAA dataset (f)).

4 Upward mass fluxes

4.1 Absolute values

For a more comprehensive overview the full zonal average updraft mass fluxes are shown in this figure in contrast to the 30 degrees binned values in the manuscript.

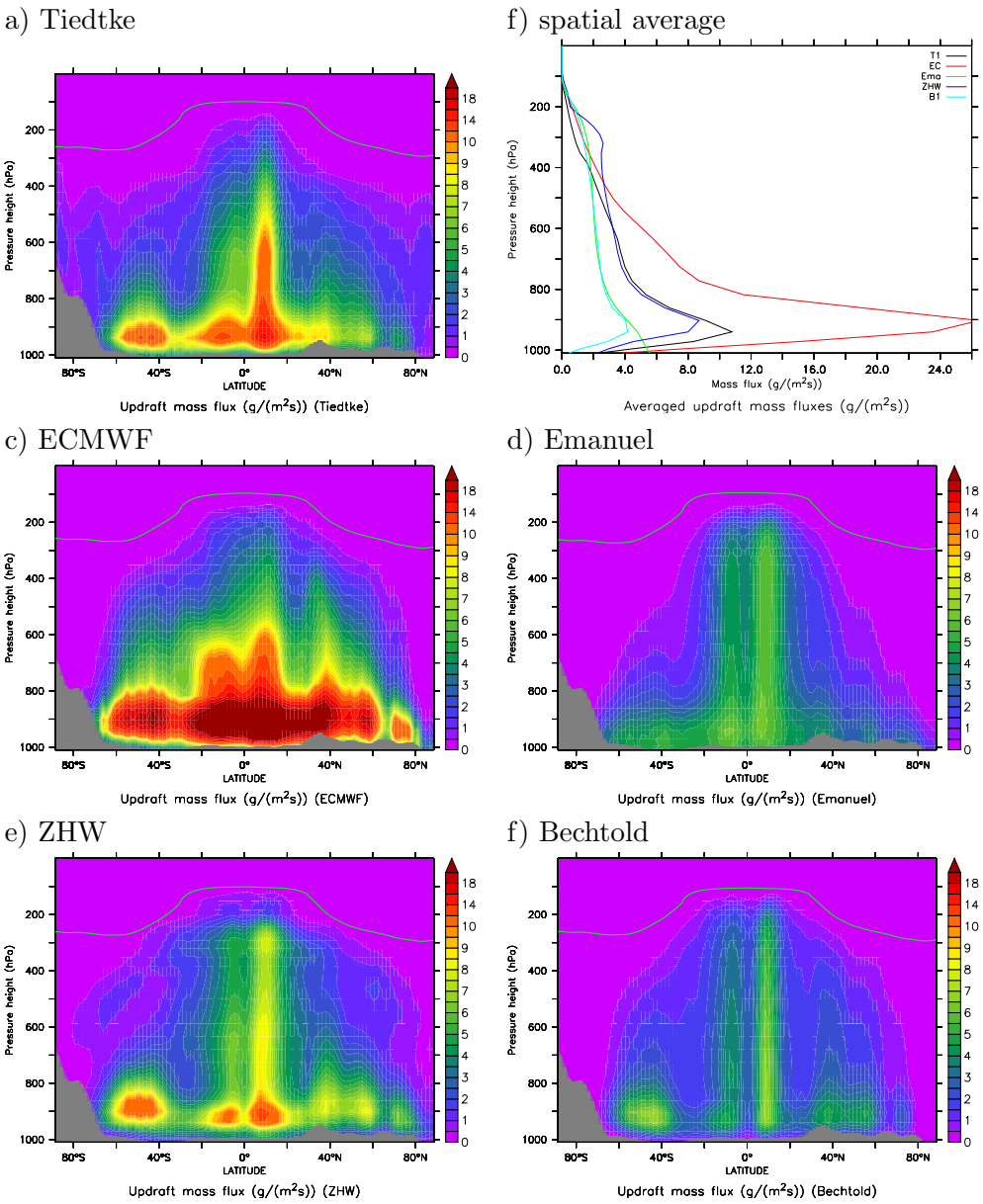

Figure 4: 4 months average of the zonal averaged convective updraft mass fluxes (a) for the T1 simulation , b) the average vertical profile. The values for the other simulations are shown in panels c)-f). The dark line denotes the tropopause and the grey shaded area the zonal mean orography.

4.2 Relative differences

To address the differences in the updraft mass fluxes this figure contains the relative differences compared to the T1 reference.

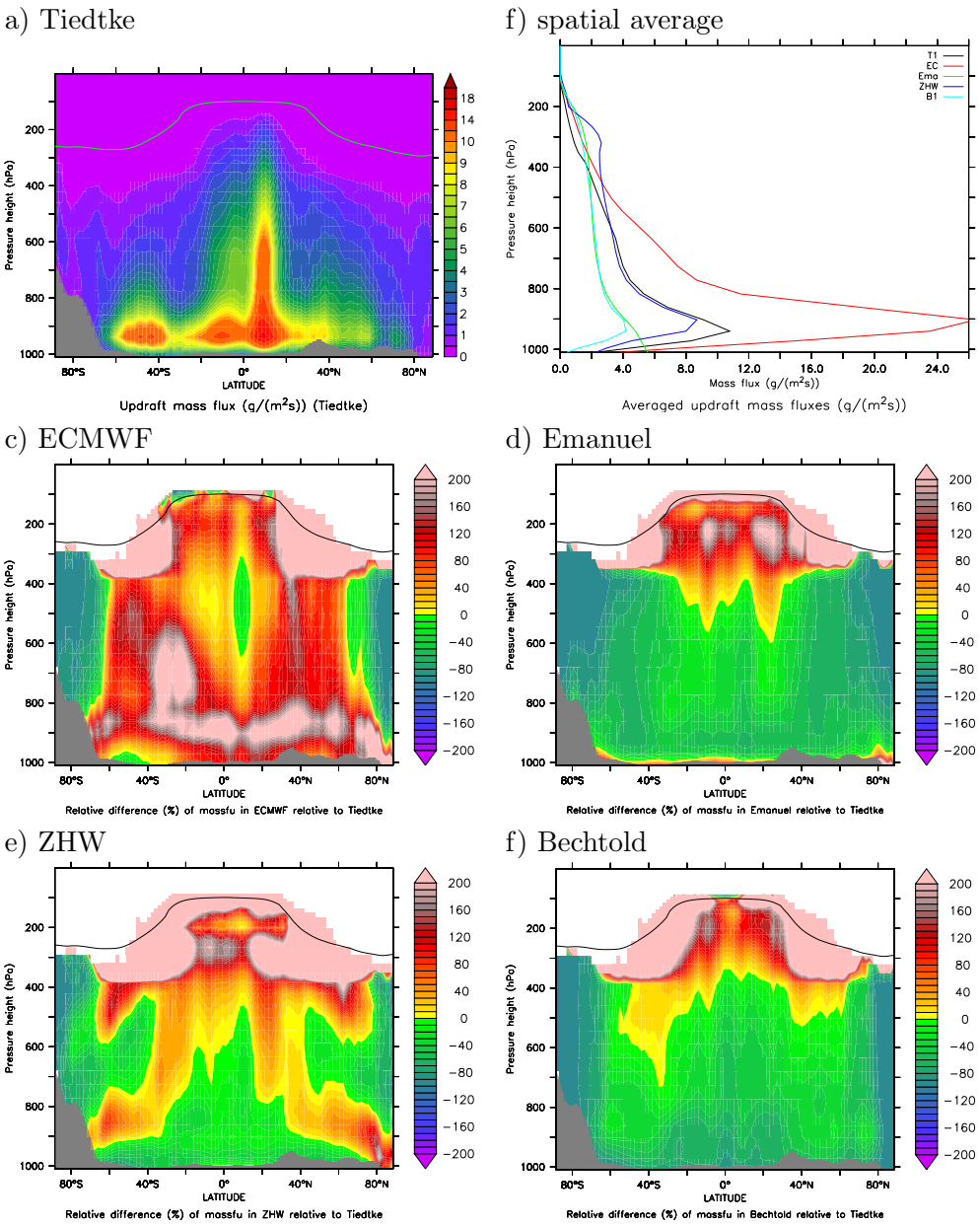

Figure 5: 4 months average of the zonal averaged convective updraft mass fluxes (a) for the T1 simulation , b) the average vertical profile. The relative differences to T1 (in %) are shown in panels c)-f). The dark line denotes the tropopause and the grey shaded area the zonal mean orography.

4.3 Frequency distributions

In addition to the vertically averaged mass flux shown in the main manuscript the frequency distribution of the updraft mass fluxes at various altitudes are shown in the following graphic.

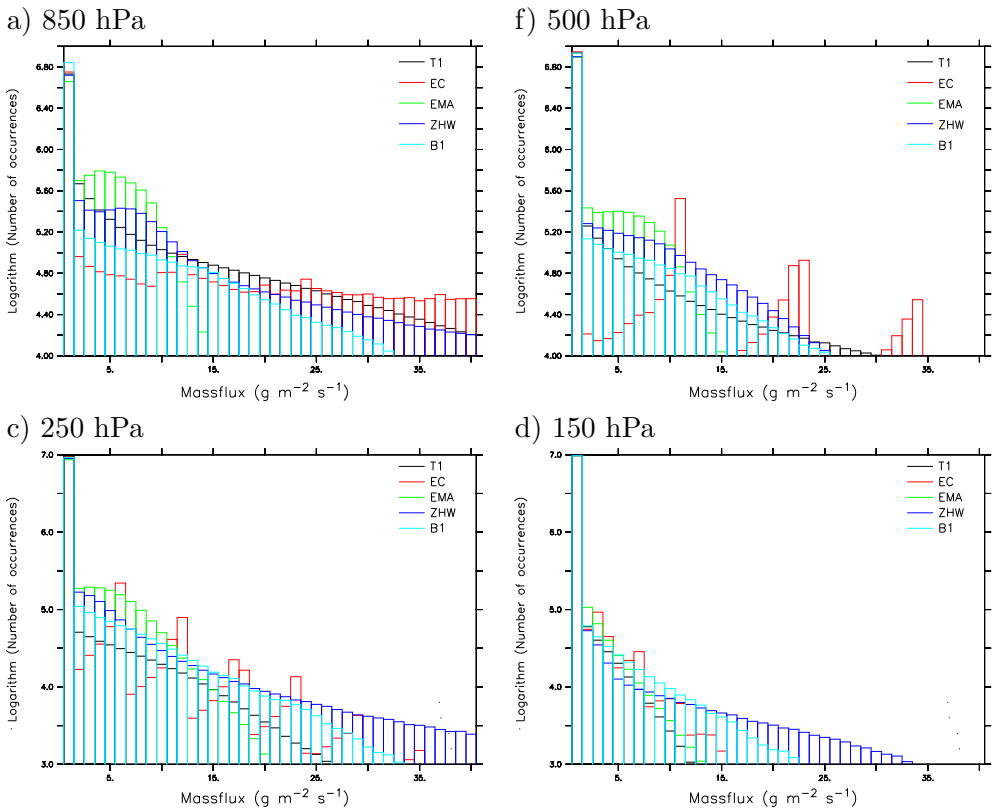

Figure 6: 4 months frequency distribution of the convective updraft mass fluxes (a) at 850 hPa , b) at 500 hPa, c) at 250 hPa and d) at 150 hPa).

5 Downward mass fluxes

In addition to the upward convective mass fluxes, the downdraft mass fluxes play an important role in downward transport of species from the upper and mid troposphere into the boundary layer. This can both be species enriched in the UTLS region, but also clean air. pollutant loading. Fig. 7 shows the downdraft mass fluxes for the individual simulations.

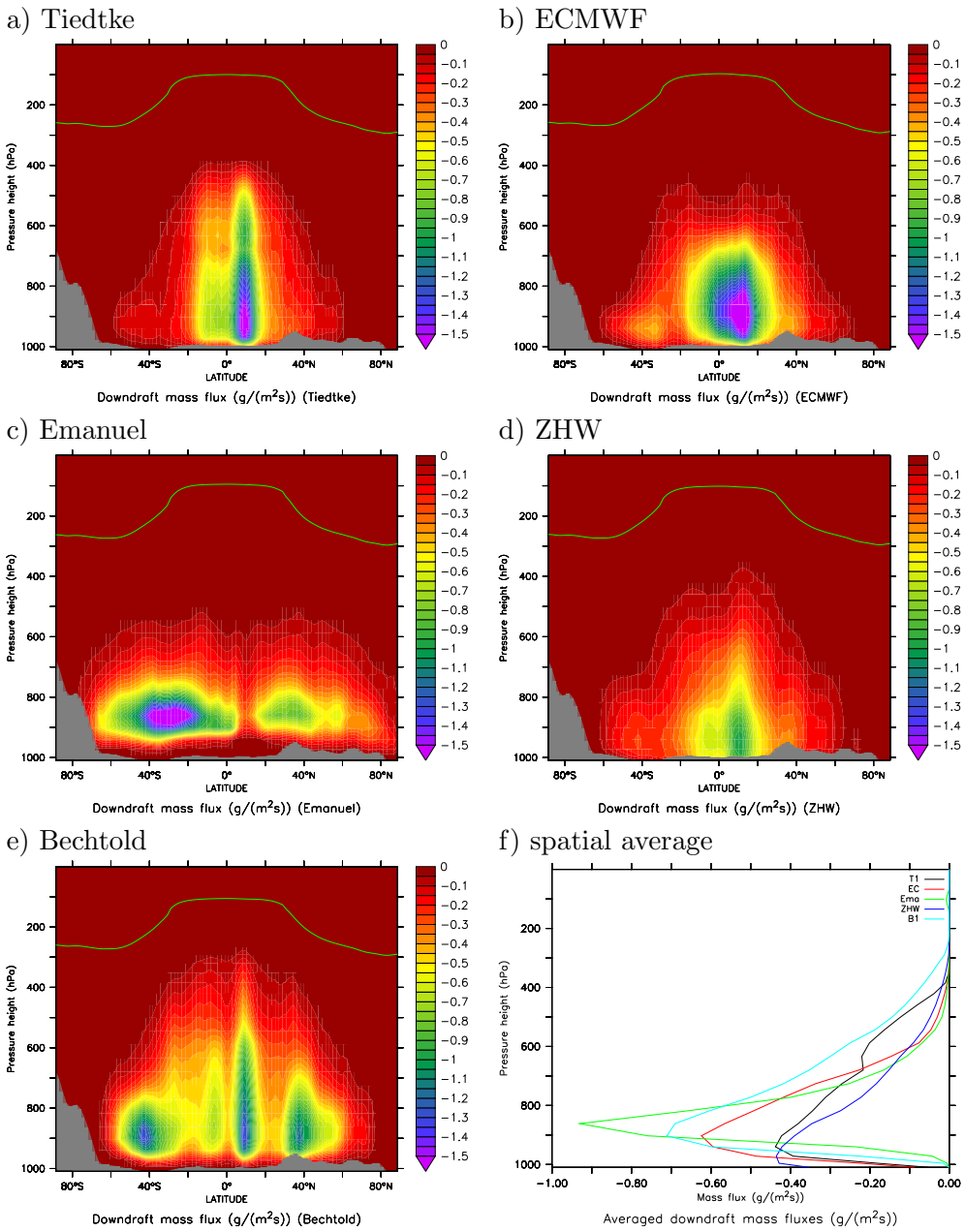

Figure 7: 4 months average of the zonal averaged convective downdraft mass fluxes (a-e) and average vertical profile (f). The green line denotes the tropopause and the grey shaded area the zonal mean orography. The negative values indicate the downward motion of the air.

6 Chemical species

6.1 OH

Since OH is the main oxidant some of the differences in oxidised compounds analysed in the main document can be better understood with the help of the analysed differences in the hydroxy radical distributions.

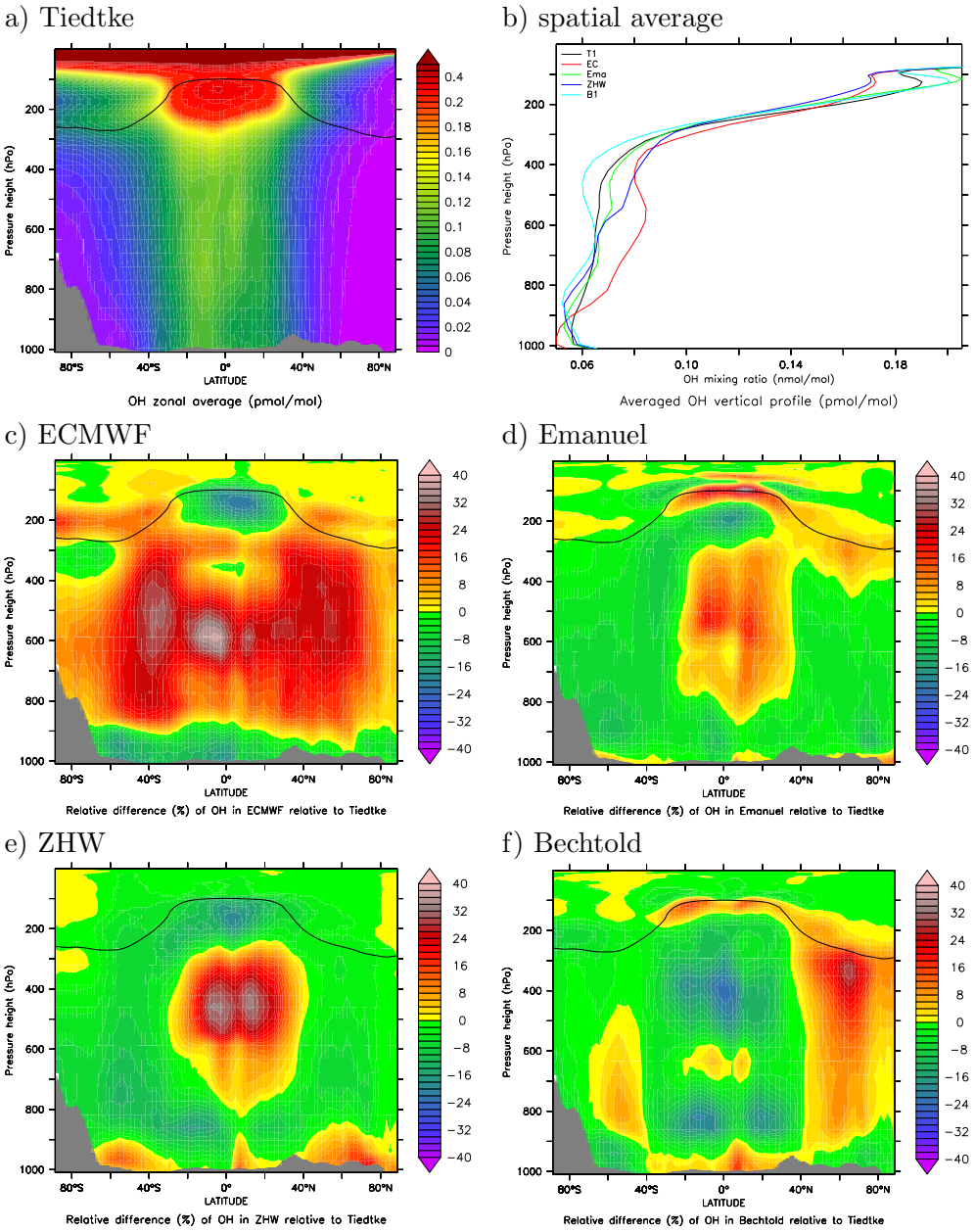

Figure 8: 4 months average of the zonal mean OH (in pmol/mol) (a), and the average vertical profile (in pmol/mol) in the five simulations(b). Panels c) to f) depict the relative difference in % with Tiedtke as the reference: $((X - T1)/T1 \cdot 100)$. The black line denotes the tropopause and the grey shaded area the zonal mean orography.

6.2 H_2O

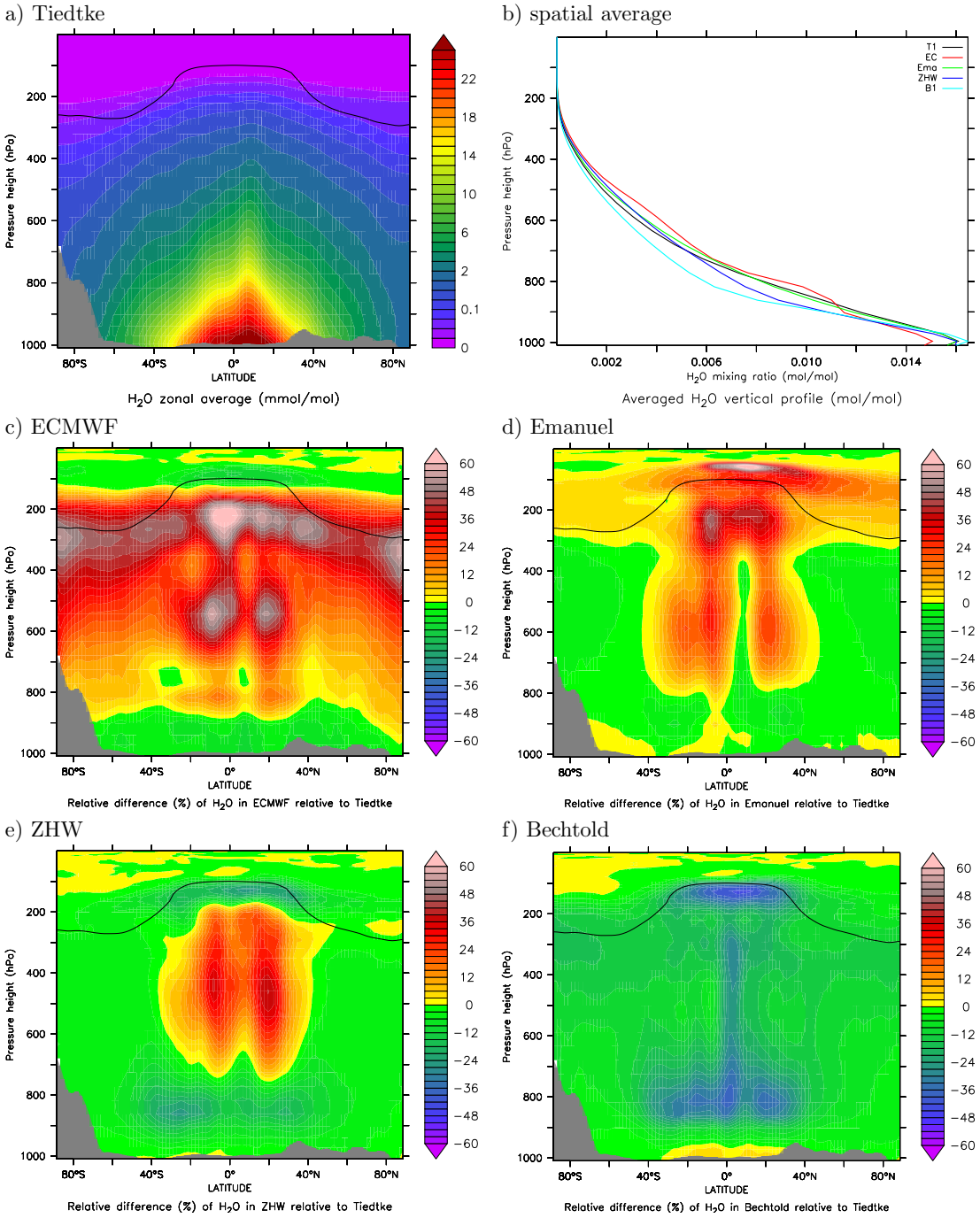

Figure 9: 4 months average of the zonal mean H_2O (in mmol/mol) **(a)**, and the average vertical profile (mol/mol) in the five simulations **(b)**. Panels **(c)** to **(f)** show the relative differences (in %) with Tiedtke as reference: $((X-T1)/T1 \cdot 100)$. The black line denotes the tropopause and the grey shaded area the zonal mean orography.

6.3 ^{222}Rn

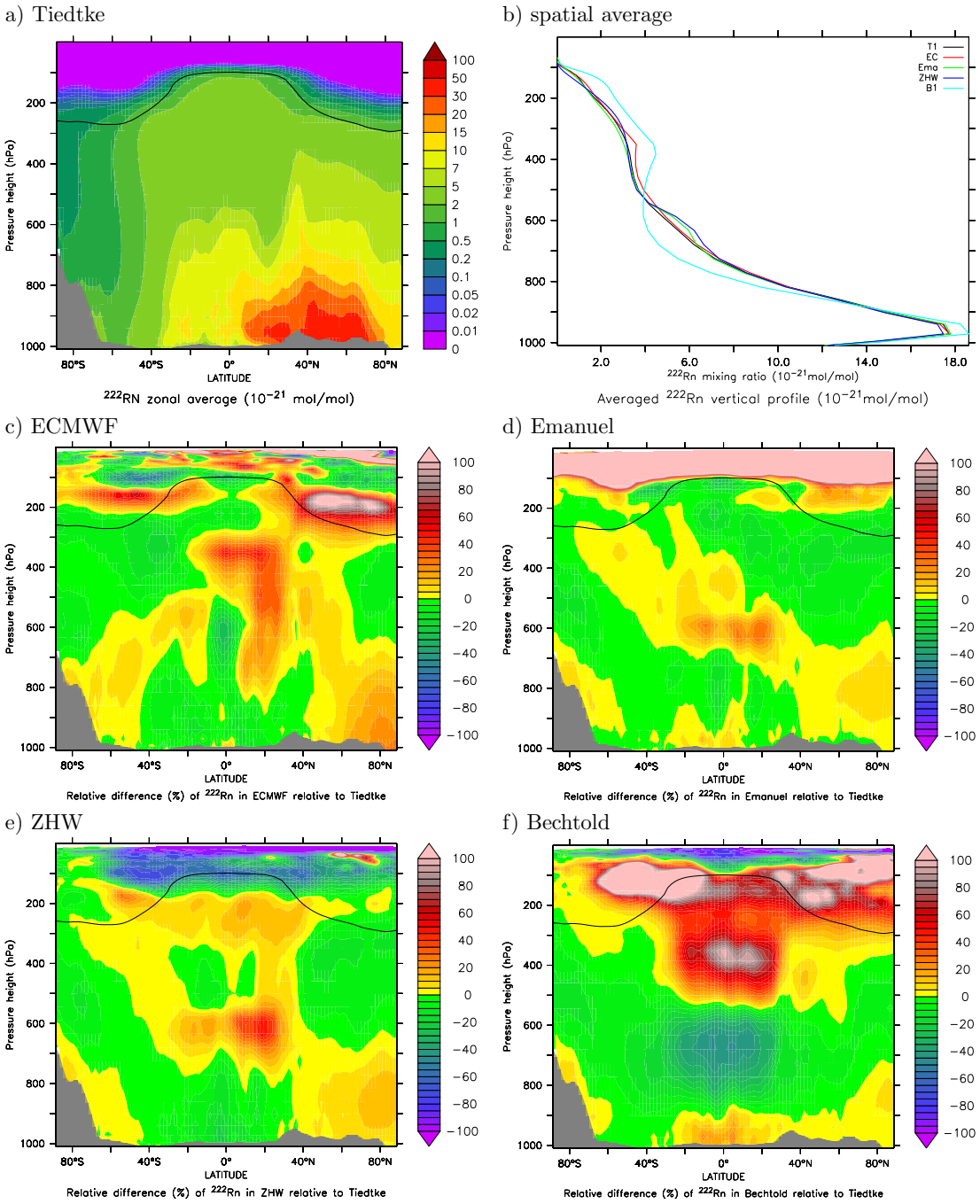

Figure 10: 4 month average of the zonal mean ^{222}Rn (in 10^{-21}mol/mol) **(a)**, and the average vertical profile (10^{-21}mol/mol) in the five simulations **(b)**. Panels **(c)** to **(f)** depict the relative differences (in %) with Tiedtke as the reference: $((X-T1)/T1 \cdot 100)$. The black line denotes the tropopause and the grey shaded area the zonal mean orography.

6.4 CO

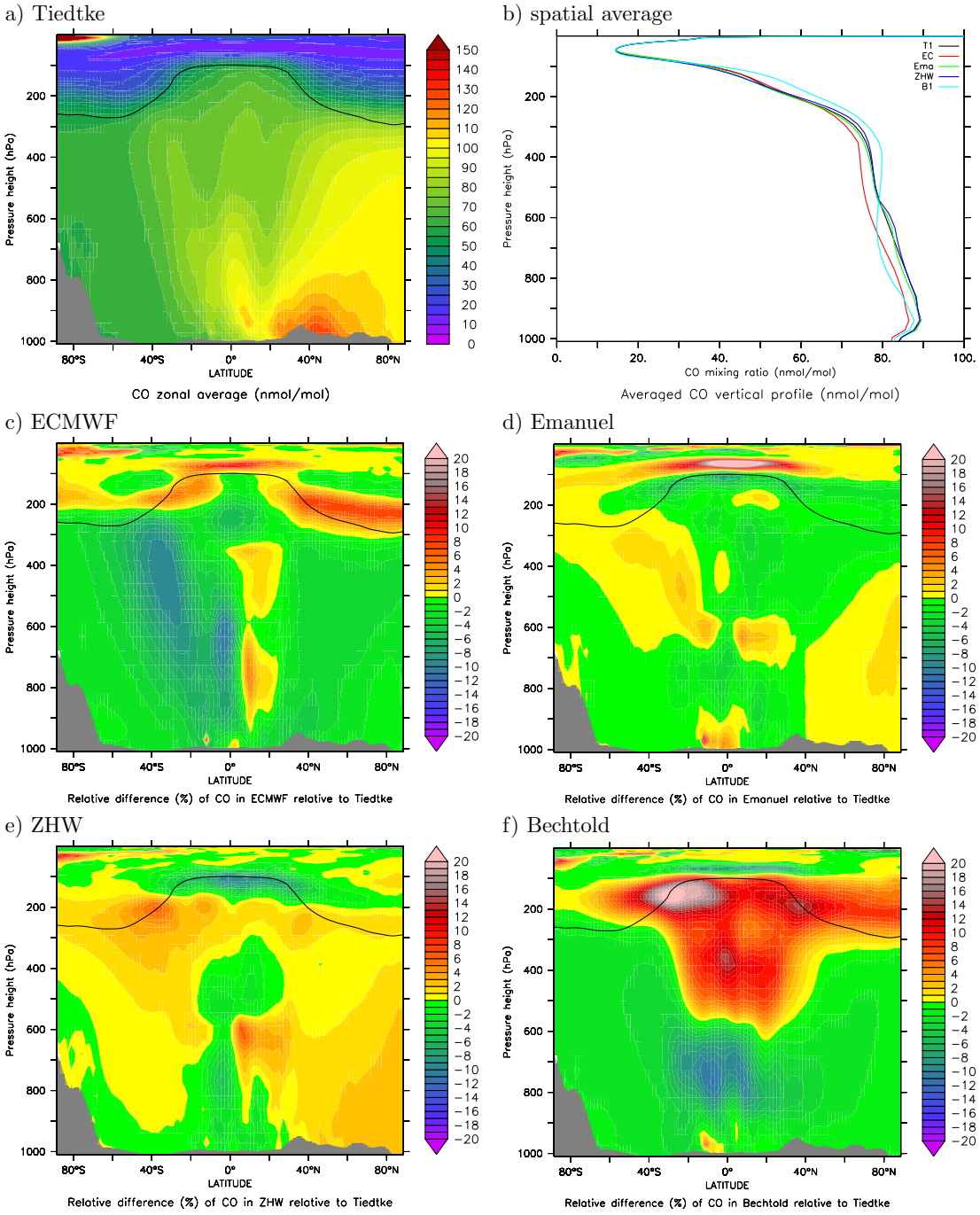

Figure 11: 4 months average of the zonal mean CO (in nmol/mol) **(a)**, and the average vertical profile (nmol/mol) in the five simulations **(b)**. Panels **(c)** to **(f)** depict the relative differences (in %) with Tiedtke as the reference: $((X-T1)/T1 \cdot 100)$. The black line denotes the tropopause and the grey shaded area the zonal mean orography.

6.5 HCHO

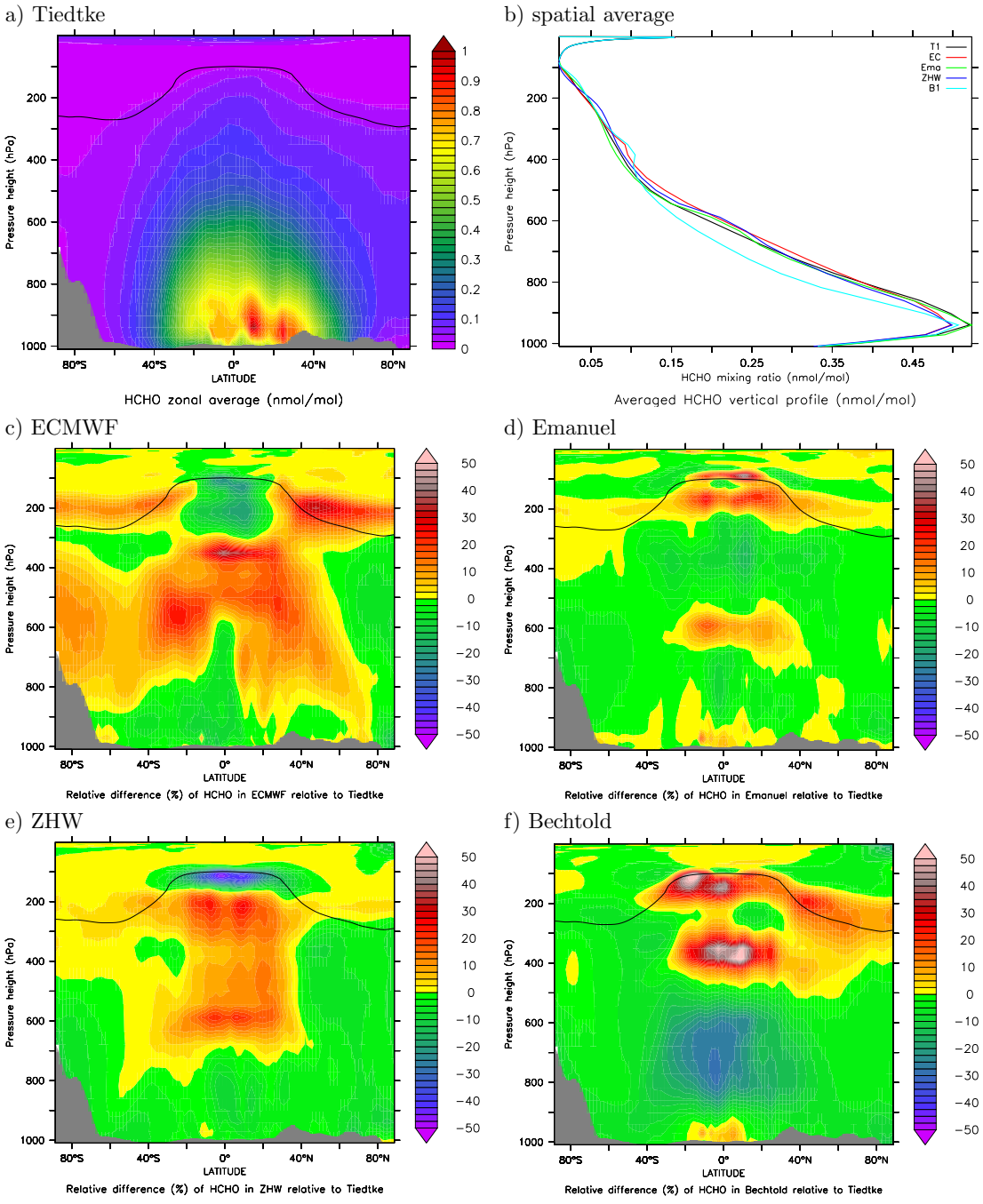

Figure 12: 4 month average of the zonal mean HCHO (in nmol/mol) **(a)**, and the average vertical profile (in nmol/mol) in the five simulations **(b)**. Panels **(c)** to **(f)** depict the relative differences (in %) with Tiedtke as the reference: $((X-T1)/T1 \cdot 100)$. The black line denotes the tropopause and the grey shaded area the zonal mean orography.

6.6 HNO_3

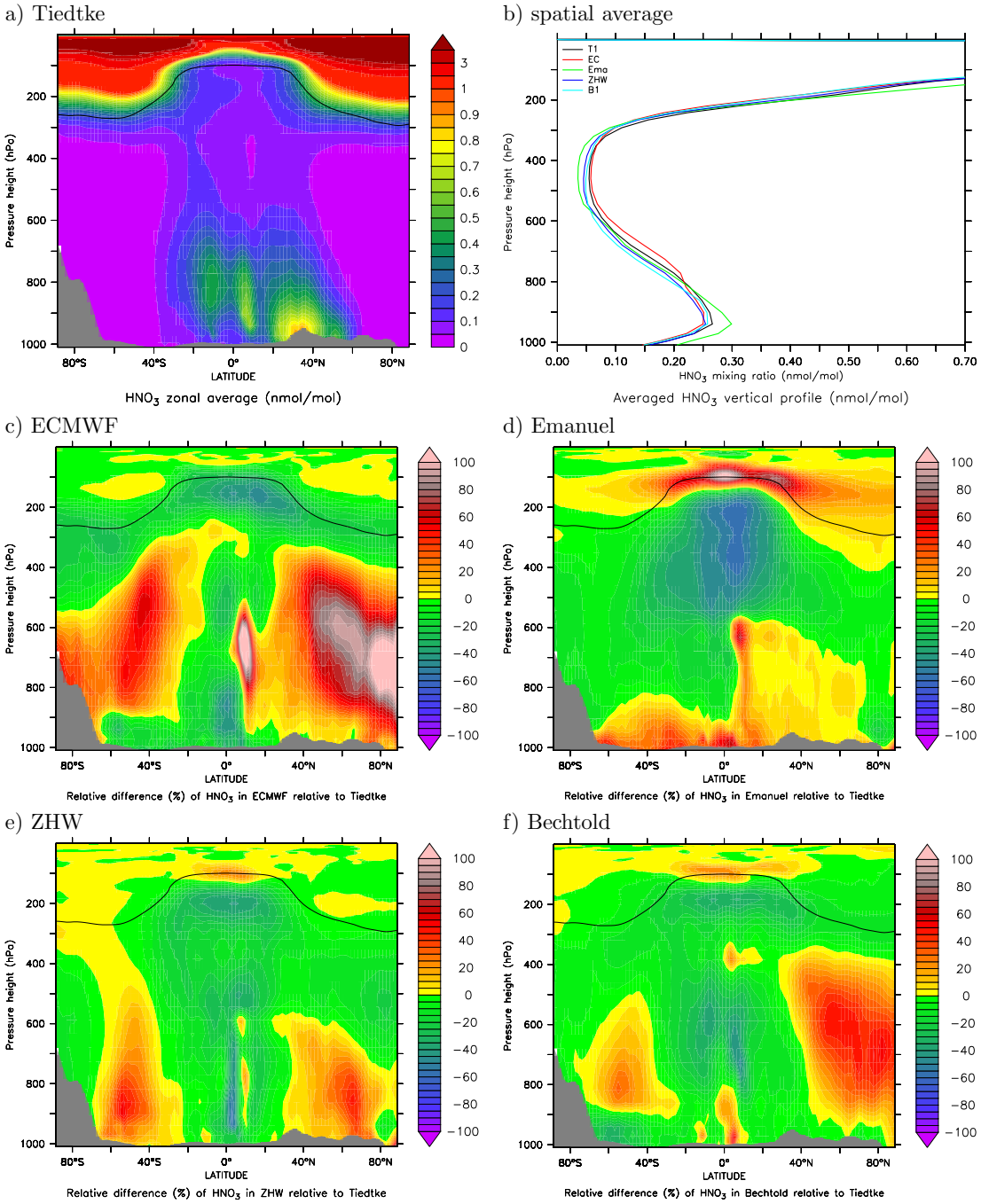

Figure 13: 4 month average of the zonal mean HNO_3 (in nmol/mol) **(a)**, and the average vertical profile (in nmol/mol) in the five simulations **(b)**. Panels **(c)** to **(f)** depict the relative differences (in %) with Tiedtke as the reference: $((X-T1)/T1 \cdot 100)$. The black line denotes the tropopause and the grey shaded area the zonal mean orography.

6.7 O_3

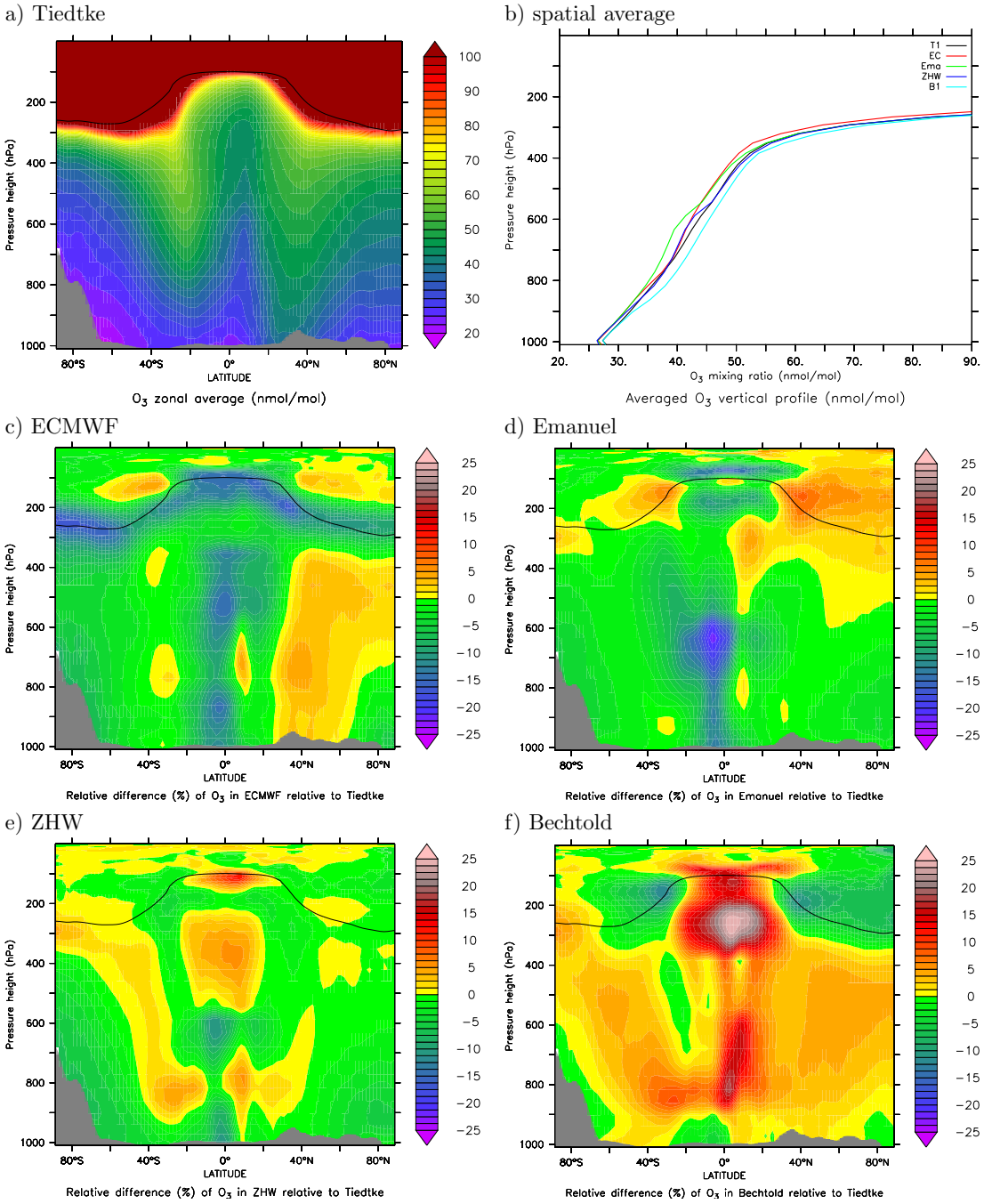

Figure 14: 4 months average of the zonal mean O_3 (in nmol/mol) **(a)**, and the average vertical profile (in nmol/mol) in the five simulations **(b)**. Panels **(c)** to **(f)**) depict the relative differences (in %) with Tiedtke as the reference: $((X-T1)/T1 \cdot 100)$. The black line denotes the tropopause and the grey shaded area the zonal mean orography.

7 Comparison with the Emmons et al. (2000) database

Some exemplary vertical profiles of campaign means and the corresponding vertical profiles from the simulations are presented here.

a) H_2O profiles

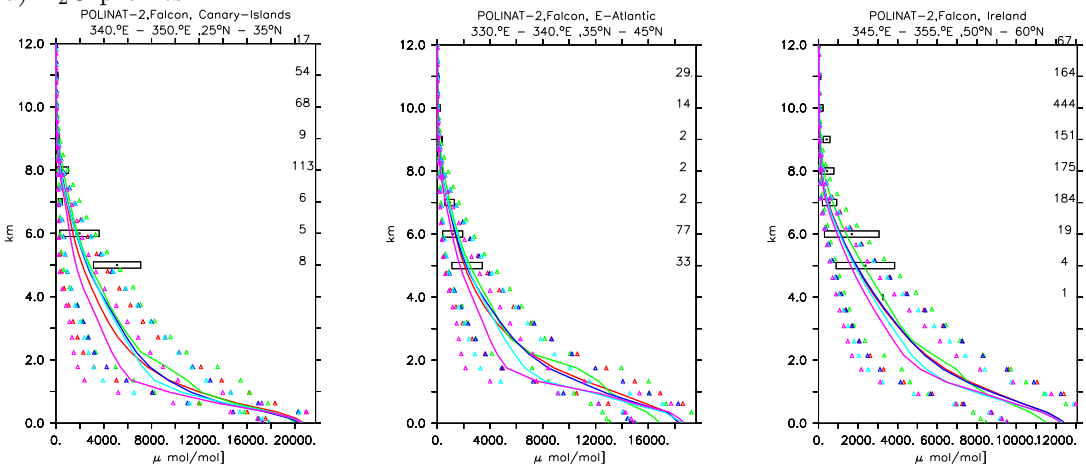

b) CO profiles

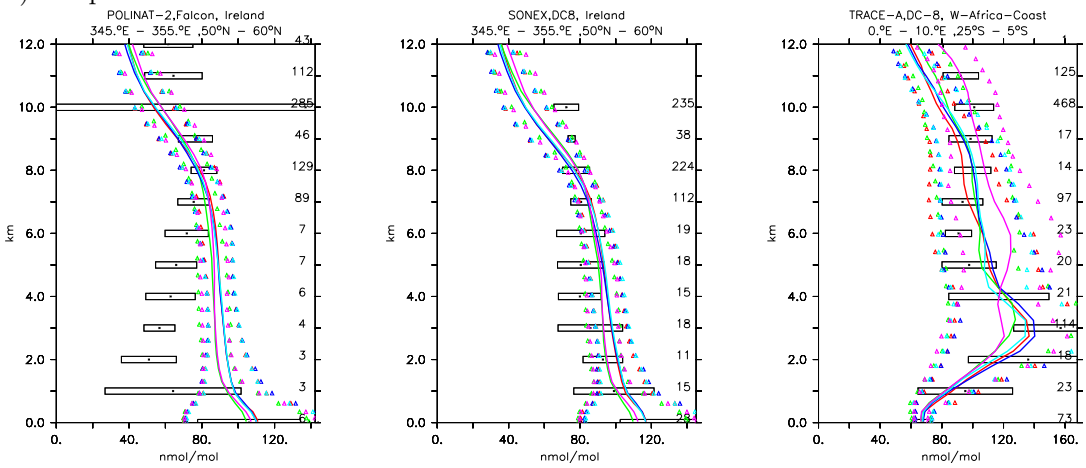

c) HCHO profiles

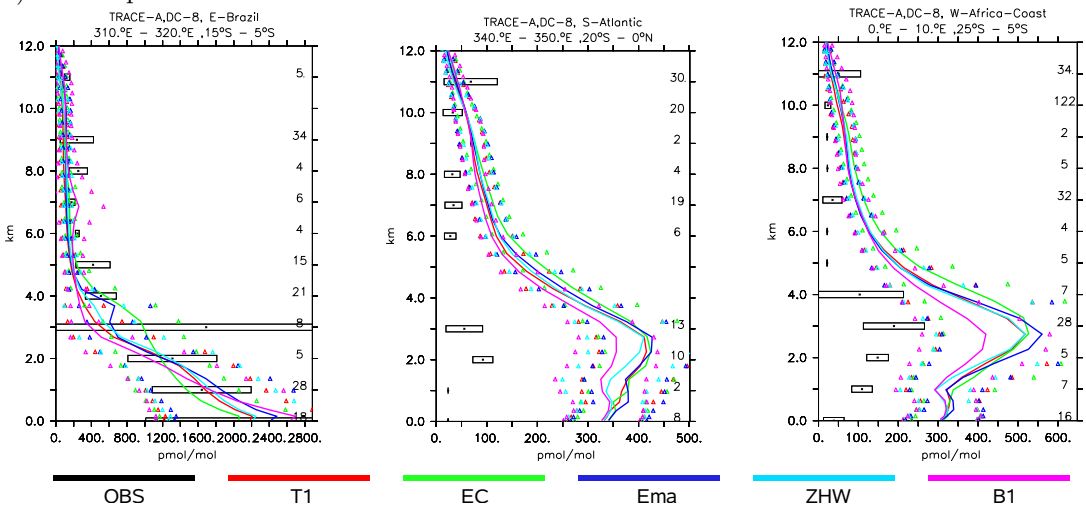

d) HNO_3 profiles

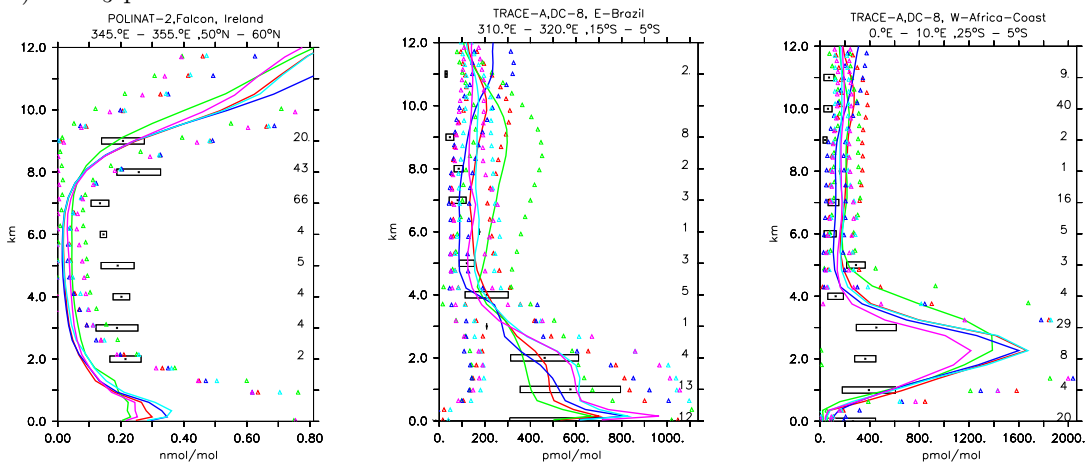

e) O_3 profiles

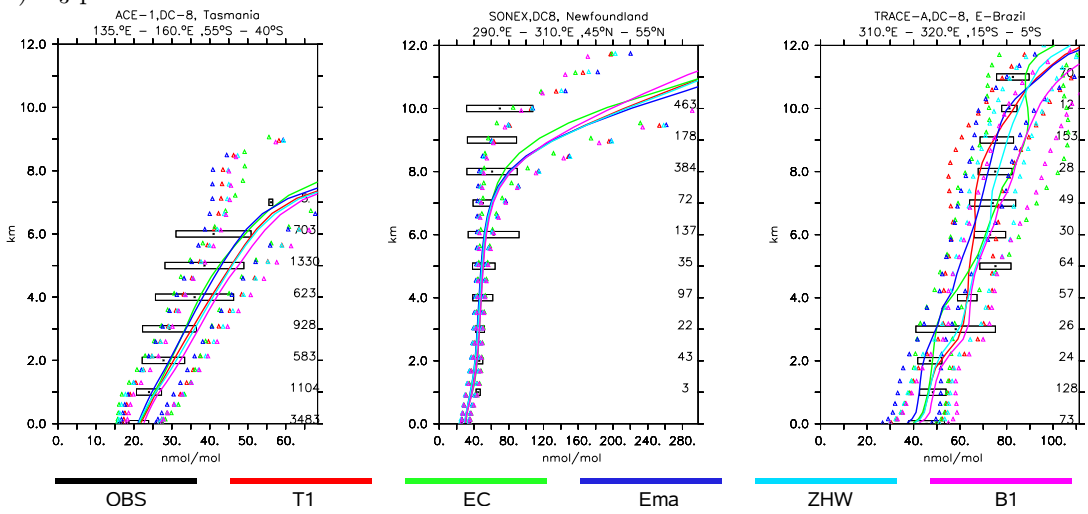

Figure 15: Vertical profiles of 5 species (a)H_2O, b)CO, c)HCHO, d)HNO_3, e)O_3) of campaign and regional means as taken from the (updated) Emmons et al. (2000) database. The black crosses represent the model mean, the black boxes the standard deviations; the coloured lines depict the model mean, sampled in the observation region, and the triangles the corresponding model standard deviation. The numbers at the right vertical axis denote the number of individual observations.

Table 2: Biases (in units of standard deviation) and linear regression (y = SLOPE $*$ x + INTERCEPT) for the comparison of the simulations using the different convection schemes with the Emmons et al. (2000) database. The intercept is in nmol/mol, except for H_2O (μmol/mol).

Compound	Quantity	T1	EC	Ema	ZHW	B1
O_3(all)						
	Bias	0.31	0.29	0.22	0.35	0.52
	Slope	1.96	1.87	2.06	1.89	1.76
	Intercept	-30.1	-30.1	-36.0	-27.1	-18.6
$O_3(< 9\text{km})$						
	Bias	0.13	0.17	0.03	0.18	0.37
	Slope	0.75	0.73	0.75	0.79	0.78
	Intercept	21.5	19.8	20.2	20.0	22.4
H_2O						
	Bias	-2.11	-1.64	-1.96	-2.11	-2.39
	Slope	0.56	0.64	0.61	0.61	0.46
	Intercept	577	1186	476	389	542
HCHO						
	Bias	0.82	1.05	0.86	0.90	0.88
	Slope	0.61	0.62	0.68	0.64	0.59
	Intercept	0.15	0.18	0.15	0.15	0.13
HNO_3						
	Bias	-0.15	0.01	-0.37	-0.13	-0.16
	Slope	0.64	0.54	0.69	0.68	0.53
	Intercept	0.12	0.16	0.08	0.10	0.10
CO						
	Bias	-0.58	-0.68	-0.61	-0.58	-0.43
	Slope	0.35	0.39	0.39	0.36	0.41
	Intercept	51.9	47.6	49.1	52.1	49.1

Table 3: Pearson's correlation coefficient (R^2) for the GABRIEL campaign.

Compound	T1	EC	Ema	ZHW	B1
O_3	0.17	0.25	0.50	0.47	0.42
H_2O	0.83	0.81	0.89	0.85	0.80
HCHO	0.19	0.20	0.18	0.16	0.17
CO	0.09	0.09	0.12	0.06	0.15

Table 4: Biases (in units of standard deviation) and Pearson's correlation coefficient (R^2) for the SCOUT-O3/ACTIVE campaign in Darwin.

Compound	Quantity	T1	EC	Ema	ZHW	B1
O_3(Geophysica)						
	Bias	0.15	0.47	0.19	0.52	0.29
	R^2	0.69	0.79	0.59	0.65	0.62
O_3(Dornier)						
	Bias	0.48	1.49	1.02	1.73	0.59
	R^2	0.22	0.47	0.18	0.49	0.23
CO(Dornier)						
	Bias	-1.21	-0.79	-0.88	-0.77	-1.53
	R^2	-0.17	-0.77	0	0.27	0.45
CO(Geophysica)						
	Bias	-1.78	-0.76	-1.74	-1.78	-1.19
	R^2	0.77	-0.04	0.57	0.45	0.93
CO(Egrett)						
	Bias	-1.77	-1.44	-1.72	-1.38	-1.91
	R^2	0.96	0.97	0.97	0.96	0.94
H_2O(Geophysica)						
	Bias	0.36	-0.55	1.20	0.57	-0.14
	R^2	0.99	0.99	0.99	1.00	1.00
H_2O(Falcon)						
	Bias	0.09	-0.79	-0.01	-0.04	0.20
	R^2	0.99	0.99	0.99	0.99	0.99
NO(Falcon)						
	Bias	-0.72	-0.44	-0.90	-1.18	-1.46
	R^2	0.97	0.77	0.89	0.97	0.95
SO_2(Falcon)						
	Bias	-1.79	-1.79	-1.43	-1.64	-1.49
	R^2	0.44	0.67	0.69	0.47	0.72

8 Wet deposition

The detailed wet deposition fluxes for nitrate and sulphate and the respective differences to the reference simulation are added, helping to estimate the differences in the tracer distributions due to scavenging and wet removal processes.

8.1 Nitrate

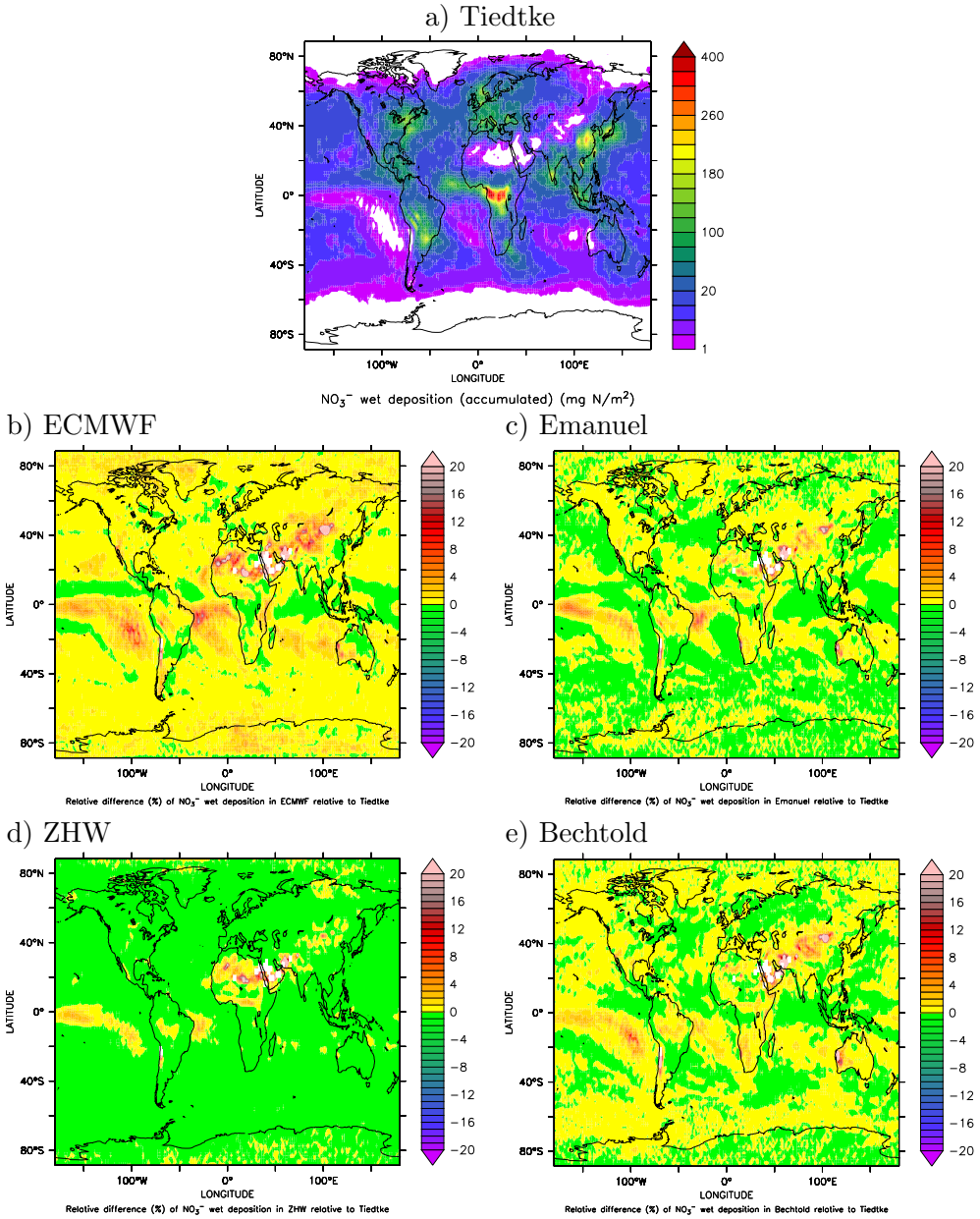

Figure 16: 4 months accumulated nitrate wet deposition flux at the surface (in mg N / m^2) for the T1 simulation (a) and relative differences (in %) of the other simulations to the T1 simulation (b) to e)).

8.2 Sulphate

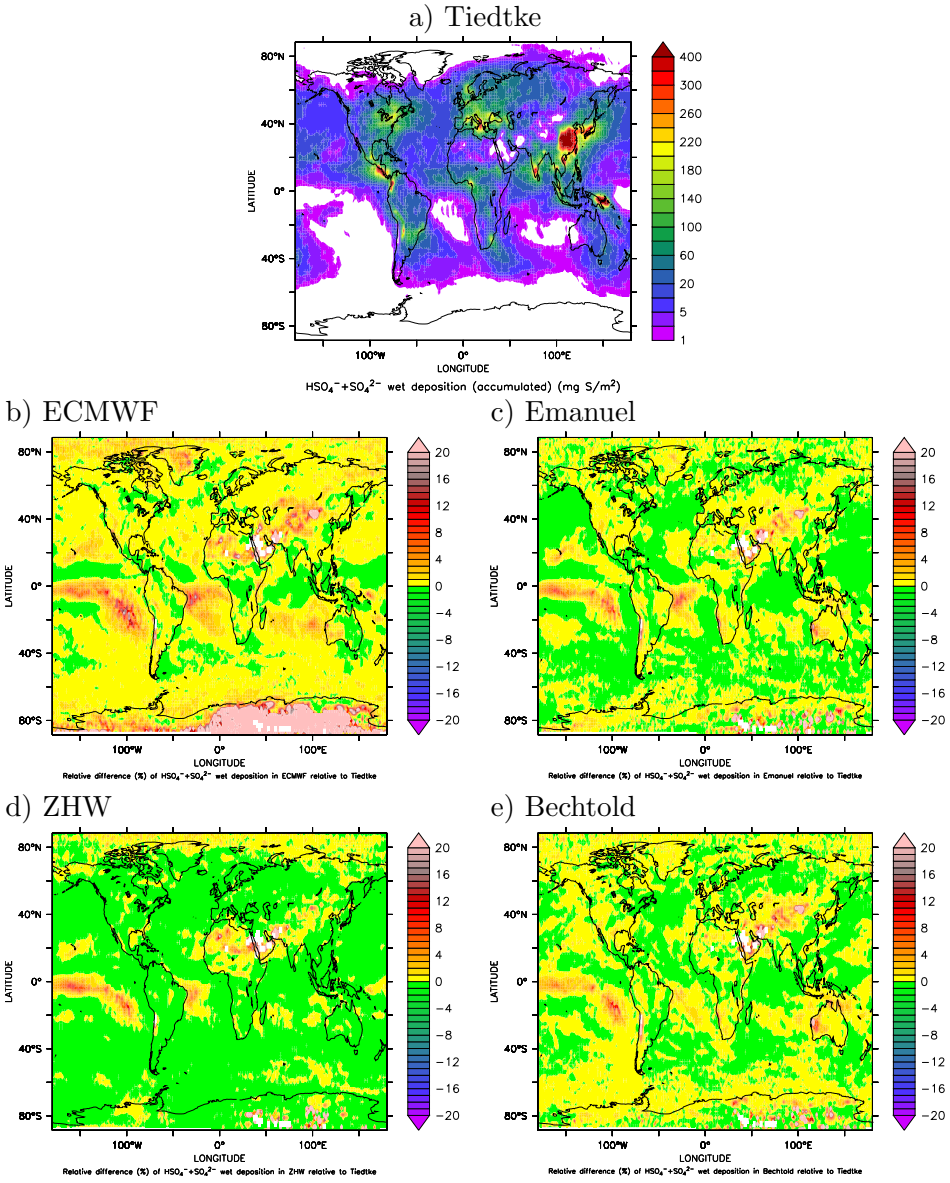

Figure 17: 4 months accumulated sulphate wet deposition flux at the surface (in mg S / m^2) for the T1 simulation (a) and relative differences (in %) of the other simulations to the T1 simulation (b) to e)).

Additionally, table 5 lists the linear regression and Pearson's correlation coefficients using the same observational data as in Tost et al. (2007) is provided for nitrate (upper) and sulphate (lower).

References

Emmons, L. K., Hauglustaine, D. A., Müller, J.-F., carroll, M. A., Brasseur, G. P., Brunner, D., Staehelin, J., Thouret, V., and Marenco, A.: Data composites of airborne

Simulation	Correlation (R^2)	slope	intercept
T1	0.29	0.43	76.02
EC	0.31	0.46	93.94
Ema	0.26	0.43	93.29
ZHW	0.20	0.19	52.49
B1	0.20	0.39	98.65
Simulation	Correlation (R^2)	slope	intercept
T1	0.29	0.40	113.9
EC	0.37	0.44	119.9
Ema	0.32	0.42	136.2
ZHW	0.32	0.31	92.8
B1	0.30	0.35	129.0

Table 5: Pearson's correlation and linear regression of simulation results (scaled to annual values) for comparison with observations (annual values) for nitrate and sulphate.

observations of tropospheric ozone and its precursors, J. Geophys. Res., 105, 20 497–20 538, 2000.

Tost, H., Jöckel, P., and Lelieveld, J.: Influence of different convection parameterisations in a GCM, Atmos. Chem. Phys., 6, 5475–5493, 2006.

Tost, H., Jöckel, P., Kerkweg, A., Pozzer, A., Sander, R., and Lelieveld, J.: Global cloud and precipitation chemistry and wet deposition: tropospheric model simulations with ECHAM5/MESSy1, Atmos. Chem. Phys., 7, 2733–2757, 2007.

v. Kuhlmann, R. and Lawrence, M. G.: The impact of ice uptake of nitric acid on atmospheric chemistry, Atmos. Chem. Phys., 6, 225–235, 2006.